New Journal of Physics
The open access journal at the forefront of physics
Deutsche Physikalische Gesellschaft DPG | IOP Institute of Physics

Coupling motion of colloidal particles in quasi-two-dimensional confinement

Jun Ma[1,2] **and Guangyin Jing**[1,3]

[1] Department of Physics, Northwest University, 710069, Xian, People's Republic of China
[2] Institute for Experimental Physics I, University of Leipzig, Germany
[3] NanoBiophotonics center, National Key Laboratory and Incubation Base of Photoelectric Technology and Functional Materials, Xian, 710069, People's Republic of China
E-mail: ma.jun@uni-leipzig.de and jing@nwu.edu.cn

Received 11 February 2014, revised 28 April 2014
Accepted for publication 27 May 2014
Published 17 July 2014

New Journal of Physics **16** (2014) 073025

doi:10.1088/1367-2630/16/7/073025

Abstract

The Brownian motion of colloidal particles in quasi-two-dimensional (q2D) confinement displays a distinct kinetic character from that in bulk. Here we experimentally report dynamic coupling motion of Brownian particles in a relatively long process (~100 h), which displays a quasi-equilibrium state in the q2D system. In the quasi-equilibrium state, the q2D confinement results in the coupling of particle motions, which slowly damps the motion and interaction of particles until the final equilibrium state is reached. The process of approaching the equilibrium is a random relaxation of a many-body interaction system of Brownian particles. As the relaxation proceeds for ~100 h, the system reaches the equilibrium state in which the energy gained by the particles from the stochastic collision in the whole system is counteracted by the dissipative energy resulting from the collision. The relaxation time of this stochastic q2D system is 17.7 h. The theory is developed to explain coupling motions of Brownian particles in q2D confinement.

S Online supplementary data available from stacks.iop.org/njp/16/073025/mmedia

Keywords: colloid, quasi-two-dimensional, confinement

1. Introduction

Particles performing Brownian motion in quasi-two-dimensional (q2D) space ubiquitously exist in diverse systems in nature. These particles exhibit fundamentally different characteristics from ones in bulk because of the effects of the confinement and coupling interaction. Great potential applications have recently stimulated extensive theoretical and experimental studies in various fields: self-propelled protein swimming in lipid bilayers of biological membranes [1], hydrodynamic diffusion of elastic capsules in bounded suspension [2], hydrodynamic interactions between particles [3–5] and particles flowing [6] in a suspension confined in a q2D channel, colloidal suspension transition to glass between two quasiparallel plates [7], etc.

When a colloidal suspension is confined between two quasiparallel glass surfaces, particle diffusion slows down for the reason that the regions of cooperative motion of particles in the confined space are qualitatively different from those in the unconfined one [8]. The lower mobility mainly results from the confinement, with the dynamics of particles reducing dramatically as the separation distance (w) of the two surfaces decreases [9, 10]. The reduction of one dimension causes stronger hydrodynamic interaction between particles, the decreasing of the diffusion coefficient [10]. However, interestingly, this interaction declines with the separation (l) of the pair of particles as l^{-2}, decaying much faster than that decreasing with l^{-1} in the unconfined suspension [11].

The confinement leads to interaction among particles much greater than that in the bulk. On the other hand, the interaction and hydrodynamic coupling between Brownian particles and confined plates results in reduction of the mean squared displacement of the particles [10]. The confinement also produces translational symmetry breaking of the suspension, thus the momentum of the suspension is not conserved where the distance is larger than w. The transverse momentum is a dominant contribution to the hydrodynamic interaction between the pair of particles in the bulk suspension, but is restrained in the confined one [12]. The rich distinct phenomena of particle suspension in confined geometries are however complicated and far from well understood.

The previous studies of the confinement mainly reveal the 'direct' effect of the dimension reduction from 3D to q2D (e.g. the suspension in bulk being confined in q2D) on the particle motion. Other than this 'direct' effect, here we study the dynamic coupling of particle motions in q2D. The motivation of this study is the fact that for suspensions with the same particle fraction the collision rate of particles in q2D is much larger than that in 3D. In this work, we report an experimental finding on the existence of a quasi-equilibrium state of Brownian particles in a q2D system. Furthermore, we show the coupling motions for the particles, and develop the theory to describe their effect on Brownian motion.

2. Experiment and theoretical model

A dilute colloidal suspension (volume fraction 1%) with a particle diameter of 1.39 μm is confined between two parallel quartz plates whose separation distance w is 7.75 μm. Heavy water is mixed into the suspension to eliminate the gravity effect. The motions of particles are observed and recorded by using optical microscopy under ambient conditions. The trajectories of particles are analyzed from the video by particle-tracking techniques [13] (see appendix A for more experimental details).

Brownian motion of a free particle in the Ornstein–Uhlenbeck process is analyzed from the Langevin equation [14],

$$\frac{\mathrm{d}v}{\mathrm{d}t} + \beta v = A(t) \tag{1}$$

in which the friction coefficient $\beta = 6\pi\eta_s r/m$ (η_s, viscosity of the suspension; r, particle radius; m, inertial mass of particle), v is the particle velocity, t time, and $A(t) = F/m$. F is the stochastic force with zero mean, $\langle F(t)\rangle = 0$, and its values are uncorrelated at different times (t, t'), $\langle F(t)F(t')\rangle = 12\pi\eta_s r k_B T\delta(t - t')$, k_B is the Boltzmann constant, T temperature, and $\delta(t)$ the Dirac delta function.

Particles performing Brownian motion in the suspension under an external force are described by Uhlenbeck and Ornstein as [14]

$$\frac{\mathrm{d}v}{\mathrm{d}t} + \beta v = A(t) + \frac{K(x)}{m}, \tag{2}$$

where $K(x)$ is the external force.

Considering that colloidal particles (figure 1(a)) keep performing Brownian motion (figure 1(b)) in the present q2D cell, the coupling interaction among particles results from significantly increasing collision rate (number of collisions/unit time) in q2D confinement compared with that in the bulk (see appendix B). Carbajal-Tinoco *et al* also indicated that the hydrodynamic interaction among particles in the confinement is much stronger than that in the bulk [10]. When a particle with a velocity v is approaching another one, the interaction force F_x between them varies inversely as their distance l, i.e., $F_x \propto 1/l$ [15]. Batchelor and Green further indicated that, as the two particles are nearly touching, a thin fluidic layer is produced between the two particle surfaces. The strong interaction between the two particles is enacted by stresses of large magnitude within a thin layer [15].

After the collision, the two particles move apart (figure 1(c)). The fluidic layer between the two particles thickens and then a liquid zone forms as the two particles are pushed further apart. The force driving the particles apart gradually decreases to zero until it makes the particles reach the final velocity of v' (figure 1(c)). As this collision is an inelastic collision, some of the kinetic energy of the particles is converted into thermal energy, resulting in damping the motion of the particles. The corresponding momentum change is $\Delta P = mv' - mv$. The motion damping results from the energy loss of particles during the collision process. Here, we suppose that a virtual damping force acts in a collision process as $\int f\,\mathrm{d}t = mv' - mv = m(k-1)v$, where $v' = kv$ and k is the velocity conversion ratio. Thus the damping force is $f = m(k-1)(-\mathrm{d}v/\mathrm{d}t)$ (the minus sign represents the velocity damping). In the process of approaching the equilibrium, since the velocity of the particles decays with time, the energy loss in the collision process gradually decreases, i.e. the damping force continually reduces as $f_d = m(1-k)(\mathrm{d}v/\mathrm{d}t)\,\mathrm{e}^{-\gamma t}$; γ is the damping coefficient. Substituting $K(x) = f_d$ into equation (2), we get the governing equation for the damping motion of a Brownian particle in q2D confinement,

$$\left[1 + (k-1)\,\mathrm{e}^{-\gamma t}\right]\frac{\mathrm{d}v}{\mathrm{d}t} + \beta v = A(t). \tag{3}$$

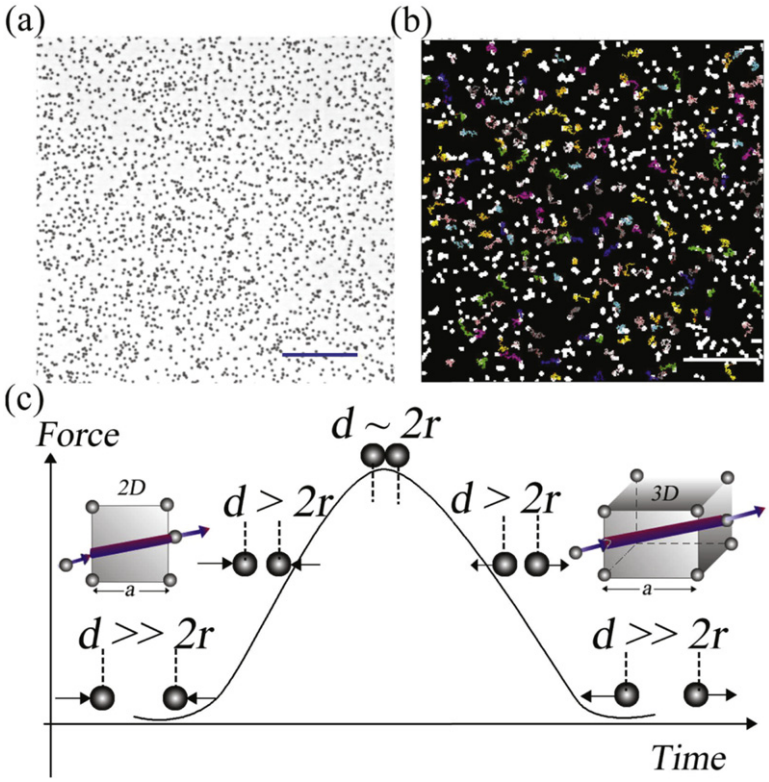

Figure 1. Particles in the suspension performing Brownian motion and colliding to produce coupling interaction. (a) Optical micrograph of the particle suspension confined in the q2D cell; the scale bar is 50 μm. (b) Typical trajectories of particle motions produced in a 16.7 ms time interval. The picture is cropped from the upper left corner of (a) with a scale bar of 10 μm. (c) Sketch of the interaction of the particles depending on their distance changing with time in the whole collision process. d continually changes to be much larger than, comparable to and equal to the particle size, which corresponds to weak, moderate and strong interaction, respectively. This is a simplified sketch of the force change between two particles during the collision process. The actual force change is much more complex. Thus the sketch does not describe the actual force but reflects the general changing tendency of the force. To qualitatively estimate the collision rate in the statistically homogenous distribution of particles in the suspension (see appendix B), a particle passing through a q2D area and 3D volume is illustrated in the left-hand and right-hand insets, respectively. The purple colour represents the scanned area and volume after the particle has passed through the q2D area and 3D volume, respectively.

The mean-square velocity $\left\langle v^2 \right\rangle$ and the mean-square displacement $\left\langle (\Delta x)^2 \right\rangle$ can be derived from equation (3) as (appendix D)

$$\left\langle v^2 \right\rangle = \frac{\alpha(t) k_B T}{m} \left(1 - e^{-2\beta t}\right) + \omega(t) v_0^2 e^{-2\beta t} \tag{4}$$

in which $\alpha(t) = \left[1 + (k-1)\,\mathrm{e}^{-\gamma t}\right]^{-2}$, $\omega(t) = \left[\frac{k}{1+(k-1)\,\mathrm{e}^{-\gamma t}}\right]^{\frac{2\beta}{\gamma}}$.

$$\left\langle (\Delta x)^2 \right\rangle = \left(\frac{kv_0}{\beta}\right)^2 \left[1 - \left(\frac{k}{\gamma t + k}\right)^{\frac{\beta}{\gamma}-1}\right]^2 + \frac{\sigma}{\beta^2\left[1 + (k-1)\,\mathrm{e}^{-\gamma t}\right]^2} \times \left[t + \frac{1}{2\beta}\left(-3 + 4e^{-\beta t} - \mathrm{e}^{-2\beta t}\right)\right] \tag{5}$$

in which $\sigma = 2\beta k_\mathrm{B} T/m$. For long time t, equations (4) and (5) turn into the equations

$$\left\langle v^2 \right\rangle = \frac{\alpha(t)\, k_\mathrm{B} T}{m} \tag{6}$$

$$\left\langle (\Delta x)^2 \right\rangle = \frac{\alpha(t)\,\sigma}{\beta^2} t. \tag{7}$$

For long time t, comparing the mean-square velocity $\left\langle v_{\mathrm{ou}}^2 \right\rangle$ and the mean-square displacement $\left\langle (\Delta x)_{\mathrm{ou}}^2 \right\rangle$ derived from equation (1) in the Ornstein–Uhlenbeck process without external force [14], $\left\langle v^2 \right\rangle$ and $\left\langle (\Delta x)^2 \right\rangle$ in equations (6) and (7) have an extra coefficient $\alpha(t)$. $\alpha(t)$ is considered as a damping factor, reflecting the damping effect resulting from coupling interaction of the particle motions. The damping factor $\alpha(t)$ decreases with increasing time t. It produces the damping effect on the double aspects: $\left\langle v^2 \right\rangle$ decreases with increasing time; $\left\langle (\Delta x)^2 \right\rangle$ increases with increasing time (t in equation (7)), but the damping factor $\alpha(t)$ lessens the increasing rate. As $t \to \infty$, $\alpha(t) \to 1$, $\left\langle v_\infty^2 \right\rangle = k_\mathrm{B} T/m$ and $\left\langle (\Delta x)_\infty^2 \right\rangle = \sigma t/\beta^2$, indicating that the damping effect finally vanishes and the coupling system of Brownian particles reaches an equilibrium.

3. Analysis of coupling motion of particles

In the present q2D cell, particles are approximately treated as a monolayer, because a particle has not been observed to pass by another particle above/beneath; instead, a collision always happens (see the videos in the supplementary material, available online at stacks.iop.org/njp/16/073025/mmedia). Particle motion is considered as lying in the X–Y plane (parallel to the two plates) due to the dimension reduction on the Z direction (perpendicular to X–Y plane). For a q2D system with the separation distance of the two plates being several times the particle diameter, the particle motion is restricted along the direction Z normal to the plates, and the particle is in a relatively 'static' state along the Z direction compared with its random motion in the 2D plane. As the particle locates close to the plate surface, the hydrodynamic stress field is asymmetric for the whole particle sphere, fields being different for the semisphere near the plate surface and the semisphere away from it. The stress field tends to bring the particle to the middle zone between the two plates for the force balance. Therefore, in the case of having no gravity effect in our system, the middle zone between the two plates is an equilibrium position

where the monolayer of particles lies. Actually, this distribution of the particles is approaching a true 2D system.

The persistent collisions inevitably result in the damping of particle motion. The ratio of the distance between the two quartz plates and particle size ($w/2r$) is 5.6, thus the viscosity of the dilute suspension is the same as that of the bulk, in terms of the experimental study of Peyla *et al* [16]. In the present system, during the slow process for approaching the equilibrium in a q2D cell, many collisions have been experienced by an individual particle. In each collision process, the energy dissipation of the particle is very small. Therefore, the coupling interaction is weak damping, so k is close to unity and γ is small. We get the root-mean-square (rms) velocity from equation (6) for the long damping process,

$$v_{\mathrm{rms}} = \sqrt{\left\langle v^2 \right\rangle} = \left[1 + (k-1)\,\mathrm{e}^{-\gamma t}\right]^{-1} \sqrt{k_{\mathrm{B}} T/m}\,. \tag{8}$$

As Einstein pointed out, the velocity and direction of particle motion change in an extremely short time, so the instant velocity can hardly be measured [17]. Here the motion of particles is measured with the absolute value of its displacement in a time interval of 16.7 ms instead. To describe the damping in the dynamic process, theoretically, a damping parameter with the character of velocity is chosen as the root-mean-square velocity shown in equation (8). Experimentally, as shown in figure 2(a), the mean (absolute value of) displacement occurs in 16.7 ms, corresponding to the velocity $V = |\Delta x|/16.7$ ms. Thus the reduction of the mean displacement can reflect the velocity decreasing in the damping process. Here, the displacements of all the particles of interest are counted. For simplicity, the counted number is normalized by the maximum value to get the value Q. The statistical result of huge quantities of trajectories displays a broad spectrum of the particle displacement Δx (figure 2(a) inset). The fitted curve in figure 2(a) reaches a plateau at about 95 h. No increasing or reducing tendency appears, but only a small fluctuation of the mean displacement. This indicates that the system reaches an equilibrium state.

The mean square displacement of particles is slowly damped with time over the very long time scale (figure 2(b)). On the other hand, on a relatively short time scale, the mean square displacement is linearly proportional to the time (figure 2(c)). This is consistent with Einstein's theory on Brownian motion, $\left\langle \Delta x^2 \right\rangle = 2Dt$, where D is the diffusion constant. The slope of the linear lines in figure 2(c) corresponds to the diffusion constant, which indicates the diffusion constant at 1 h is larger than that at 100 h. Figure 2(c) also indicates that $\left\langle \Delta x^2 \right\rangle$ at 1 h is larger than that at 100 h, which is consistent with the damping of particle motion displayed in figure 2(b). As shown in figure 2(d), a distribution centering around 80 nm consists of huge numbers of displacements and can be fitted with a Gaussian function, which is maintained during the coupling (damping) process.

Figure 2(a) indicates that the coupling interaction between particles leads to damping of particle motion. The mean displacement $\langle \Delta x \rangle$ decreases from 139 nm at the beginning (1 h) to 131 nm at equilibrium (~100 h), with a 6% reduction. Since huge numbers of trajectory steps (e.g. $\sim 10^4$) are considered here, this total reduction is a great amount, which is significant in the dynamic system. The dynamic change (fluctuation) of $\langle \Delta x \rangle$ reflected by the average of a few trajectory steps is more obvious than that done by the huge quantities of steps in figure 2(a). For the details of the analysis, see appendix C. The result of the damping is reliable for the following reasons. First, the result is based on the statistics of large numbers (e.g. $\sim 10^4$

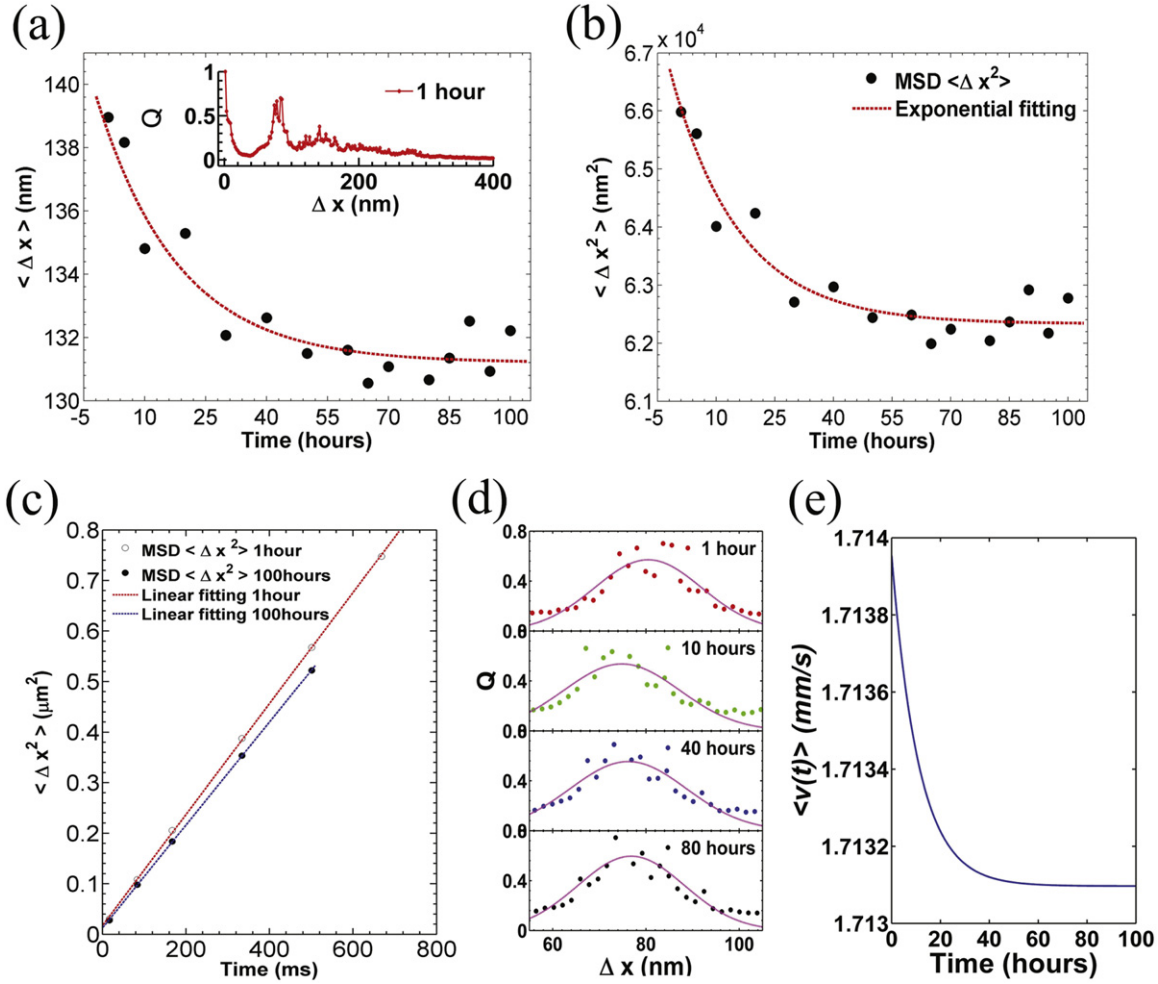

Figure 2. The dynamic change of the parameters in the coupling process. (a) The mean displacement and (b) the mean square displacement are slowly damped. $\langle \Delta x \rangle$ is calculated by dividing the sum of all displacements (absolute value) in a 16.7 ms interval by the total number of steps of all particles of interest. The starting data point is chosen at 1 h because at this time the stability is established after the suspension is sealed into the q2D cell. The red dotted line is an exponential fit. Inset is the survey spectrum of the displacement of particles at 1 h. In (a) and (d), Q is the normalized quantity. (c) The mean square displacement is linearly proportional to the time. (d) Huge numbers of displacements displays a normal distribution centering around 80 nm, showing a statistical maximum probability at a certain value. The normal distribution has been kept in the whole coupling process, which can be fitted with a Gaussian function (pink lines). (e) Theoretical predication of the velocity damping. $k = 0.9995$, $\gamma = 0.000025$.

trajectory steps of nearly 500 particles at 1 h) of the measurement. Second, from 1 h to ∼100 h, the results at all times point to damping. This indicates that the damping is not a fluctuation at a special time but a determined changing tendency. The average displacement $\langle \Delta x \rangle$ in a time interval 16.7 ms, i.e. average velocity $\langle \Delta v \rangle$, gradually decreases with the time, but the reduction rate decreases (figure 2(a)). This is consistent with the prediction from equation (8) shown in

figure 2(e). Therefore, the damping factor $\alpha(t)$ in equation (6) can describe particle motion slowly damping into the final equilibrium.

Because the instant velocity of Brownian motion is not available in the present work, here the discussion of the velocity is made on a qualitative assessment. v_{rms} in figure 2(e) refers to the instant velocity on a typical time scale, $\sim 10^{-6}$ s. However, the time scale of the average velocity corresponding to figure 2(a) is $\sim 10^{-2}$ s. The consistency in the dynamic tendency of these two velocities is manifested once the conceptions of the different time scales are reconciled. Consider a particle moving 10^4 steps with each step of time interval 10^{-6} s; the total duration is 10^{-2} s. Suppose that a 6% reduction of displacement ($\delta \langle \Delta x \rangle = 139$–$131$ nm) has been achieved by accumulation of the reduction over 10^4 steps, with the decrease of each step by 8×10^{-10} mm. Thus the velocity reduction is 8×10^{-10} mm10^{-6} s, namely, the velocity damping from 1 h to $\sim$100 h is of the order of magnitude of $\sim 10^{-4}$mms^{-1}, which agrees with the result derived from equation (8) shown in figure 2(e).

As presented in figure 2(a), the displacement tends to approach a saturated plateau, i.e. the dynamics of particles reaches the equilibrium state at $\sim$100 h. The ratio of the relative value of Δx (Q) at various times to that at $\sim$100 h is represented by the value Q_{r} (figure 3(a)), which is obtained from Q divided by the reference Q_{100} (the Q at 100 h in figure 3(b)). At the beginning (1 h), large numbers of displacements form a spectrum possessing many spike-like peaks. Thereafter (10 h), these quantities decrease, with the whole spectrum lowering towards the baseline ($Q_{\mathrm{r}} = 1$, corresponding value displayed in figure 3(b)). With the time proceeding (40 h, 80 h), the numbers of displacements larger than 200 nm continually decrease. Some fluctuation of quantities around the baseline appears at 80 h.

Most of the reduction of the numbers of displacements (>80 nm) occurs in the first 10 h, whereas a small amount of reduction is produced in the subsequent process. In fact, decreasing numbers of displacements (>80 nm) in figure 3(a) lead to the average displacement decreasing in figure 2(a). Both figures indicate that relatively quick damping occurs in the first 10 h, followed by slow damping in the subsequent coupling process.

The above description indicates the existence of a long quasi-equilibrium of Brownian particles in the q2D confinement, in which the dynamic system slowly proceeds toward the equilibrium. The stochastic force originates from the thermal fluctuation, whose effect may be considered invariant. For particles of damping motion, the friction force and coupling interaction of particles reduce as velocity decreases. In figure 2(a), the time corresponding to 1/e of the initial mean displacement is the relaxation time of 17.7 h. At the equilibrium state, on the statistical meaning for the whole q2D system of Brownian particles, the energy gained by the particles from the collision is offset by the dissipative energy resulting from the collision.

4. Trajectory analysis of particle coupling motion

In the case of a particle performing random motion in a stochastic process, Gaveau *et al* derived the equation from the statistical mechanics describing the probability density of the particle [18]. We find it is feasible to modify this equation by incorporating the damping effect, i.e., adding $e^{-\lambda t}$ (λ, damping coefficient) on both sides of the equation (for the derivation see appendix E),

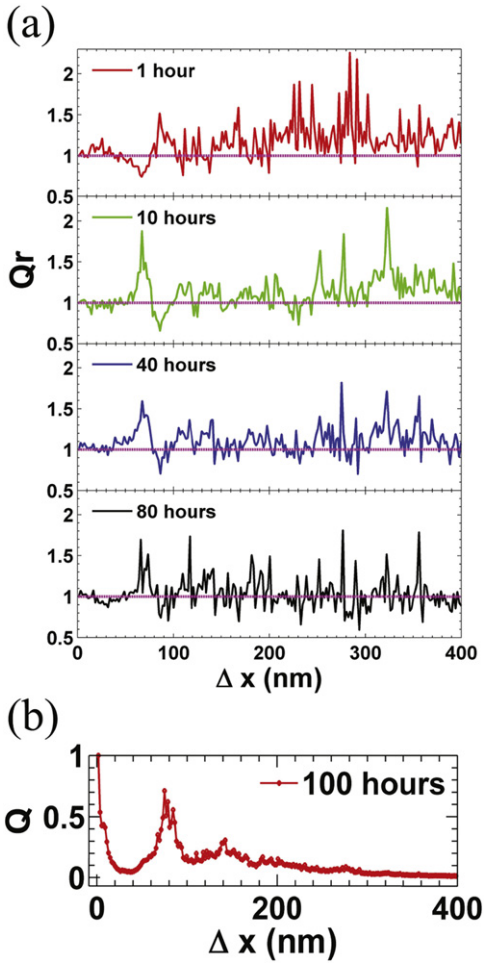

Figure 3. Distribution of the displacement (in 16.7 ms) of particles at various times. (a) Decreasing the relative number of various Δx values reflects the damping of particle motion in the coupling process. The horizontal pinkish line locating at unit value indicates the value at equilibrium. Q_r is the relative quantity, corresponding to Q at different times divided by that at 100 h in (b). The first spectrum at 1 h is acquired from figure 2(a) inset divided by figure 3(b). (b) The spectrum of the displacement of particles at equilibrium at 100 h. Q is the normalized quantity.

$$\frac{\partial^2 P}{\partial t^2} + 2a_0 \mathrm{e}^{-\lambda t}\frac{\partial P}{\partial t} = \left(v_0 \mathrm{e}^{-\lambda t}\right)^2 \frac{\partial^2 P}{\partial x^2}, \tag{9}$$

where $P(x, t)$ is the probability density of a particle appearing at position x at time t, a_0 the initial probability for the change of motion direction in unit time, and v_0 the initial velocity of the particle. Solving the equation above, we get (appendix appendix E)

$$P_n = v_0^{-1}\left[v_\mathrm{e} + (v_0 - v_\mathrm{e})\mathrm{e}^{-\rho t}\right]\mathrm{e}^{-\zeta t}\cos k_n x, \quad n = 0, 1, 2\ldots \tag{10}$$

in which $k_n = \frac{(2n+1)\pi}{2L}$ (L is the moving distance of the particle without changing direction), v_e the velocity at equilibrium, $\rho = 2\sqrt{a_0^2 - k_n^2 v_0^2}$, $\zeta = \left(a_0 - \sqrt{a_0^2 - k_n^2 v_0^2}\right)\mathrm{e}^{-\lambda t}$.

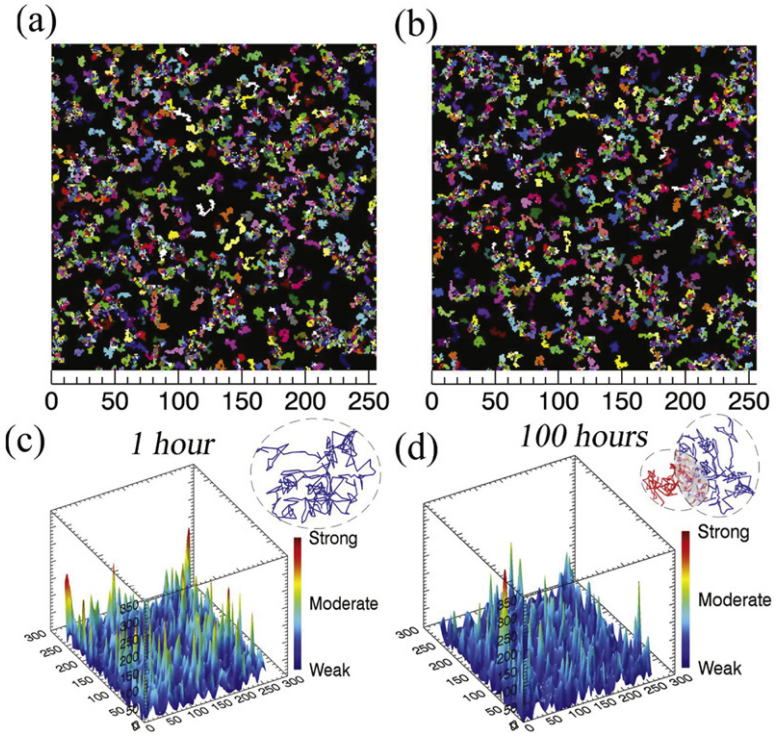

Figure 4. Coupling the motions of particles and overlapping the trajectories of motions. (a), (b) The entanglement of the trajectories of particles at 1 h and 100 h, respectively. Different colors are used to identify the trajectories for different particles. The scale bar shows the field of view of 256 × 256 pixels. (c), (d) Overlapping trajectories represented by the peaks. The higher peak corresponds to the strong overlapping of more trajectories, depicted with warm colors (yellow and even red at the peaks). The insets in (c) and (d) are the active area of an individual particle and the illustrative overlapping, respectively.

Equation (10) indicates that the probability density of the particle fluctuates in the spatial distribution. In Brownian motion, particles move in random directions. The superposition of many density fluctuations with random directions leads to the fluctuation (inhomogeneity) of particle distribution, as shown in figure 1(a). This is analogous to the works of Cahn and Vrij in spinodal decomposition [19] and spinodal dewetting [20], respectively. Cahn and Vrij showed that the superposition of fluctuations (of composition/film thickness) with random directions forms the inhomogeneous distribution of concentration [19] and thickness [20]. Particle trajectories are produced by the positions of particles accumulated in a time interval which are keeping in an inhomogeneous distribution (figures 4(a) and (b)).

A particle with a larger velocity appears in more locations in unit time, thus corresponding to the larger probability density here. Equation (10) indicates that the probability density of a particle decreases with time due to the damping, corresponding to the reduction of velocity. The damping factor ζ exponentially decreases with time, meaning that the damping effect lessens with time, which is consistent with the experimental results in figures 2(a) and 3(a).

The effect of particle interaction in the coupling process is indicated in the experimental results shown in figure 4. Analysis of the details (not obvious in figures 4(a) and (b)), shows that more trajectories of different particles (displayed by different colors) intertwine together in

figures 4(a) than in (b), indicating stronger particle interaction at 1 h than at 100 h. To quantitatively evaluate the interaction, in figures 4(c) and (d), overlapping trajectories of different particles are represented by the height. A higher peak means that more trajectories are overlapped (i.e. stronger intensity of overlapping). The heights of the peaks have reduced after a long coupling process, implying that the intensity of trajectory overlapping decreases, i.e., particle interaction is damped with time. We denote the active area of the particle as the area S enclosing the trajectories of the individual particle for a time interval Δt indicated by the dashed circle (figure 4(c) inset). The reduction of the heights of peaks results from the overlapping active area (figure 4(d) inset) decreasing, corresponding to the active area shrinking. Thus the probability of finding the particle in unit area decreases, i.e. the probability density of the particle reduces, as corroborated by equation (10). Therefore, the reduction of overlapped areas means that the intensity of particle interaction has decayed.

The changing character of particle trajectories in the solid–liquid phase transition was displayed in the pioneering work of Pierański *et al* [21]. Pierański *et al* showed that particle trajectories turned from regularity to irregularity as the solid–liquid phase transition occurred. In the solid phase, the trajectories of each particle made up a circular shape (a trajectory disc). Like atoms in a crystal, trajectory discs located on the lattice position, indicating no overlapping trajectories between particles. In contrast, the configuration of trajectories was irregular, random and overlapped in the liquid phase. Recently, Türkcan *et al* corroborated that the force acting on a Brownian particle can be derived from statistical analysis of particle trajectories [22]. The variation of the force on the particles corresponds to the different circular (or elliptical) configurations of particle trajectories.

5. Conclusion

In summary, we report the existence of a quasi-equilibrium state of Brownian particles in q2D confinement. In the quasi-equilibrium state, the confinement results in coupling particle motions, which slowly damps the mean displacement and interaction of particles. The change of the mean displacement is terminated after a relatively long process (~100 h), indicating that the quasi-equilibrium state has transited into the equilibrium one. This transition process is a random relaxation of the q2D system with Brownian particles. The relaxation time of the system is 17.7 h. In the equilibrium state, for the whole system with statistical meaning, the energy acquired by the particles from the stochastic collision is equal to the dissipative energy resulting from the collision. The theory developed here predicts the dynamic coupling motions of Brownian particles, which are consistent with the experimental result.

Acknowledgments

The authors gratefully acknowledge support from NSFC (No 111 042 18), the Scientific Research Foundation for Returned Overseas Chinese Scholars (Shaanxi Administration of Foreign Expert Affairs, 2011), SRF for ROCS, and SEM. The authors thank the anonymous reviewers for their constructive comments, which helped to improve the manuscript.

Appendix A. Experiment

Materials. A colloidal suspension of polystyrene microspheres (microParticles, Germany) was used as received. Particles were monodispersed in aqueous solution with the weight percent 10wt%. The diameter of the particles is 1.39 μm, with a standard deviation (SD) of 0.04 μm. The suspension is further diluted to 1wt% with deionized (DI) water (1.0 g ml^{-1}) with a standard resistivity of 18.29 Ωcm. To exclude the gravity effect of particles, heavy water (D_2O: density, 1.107 g ml^{-1}; purity, 99.9%; Sigma-Aldrich) and DI water are mixed to make an aqueous solution with a density of 1.05 g ml^{-1}, the same as the density of the polystyrene microspheres.

Experimental setup. Two parallel fused quartz plates (UQG Optics, UK) with the dimensions of 25 × 25 × 1 mm are placed horizontally as a q2D cell. The quartz plates are polished into a high level of uniformity of roughness and flatness by the product supplier. The root mean square roughness of both sides of the plates is characterized by atomic force microscopy (Dimension Icon, Veeco) as 0.6 nm in 10 × 10 μm area. The flatness and parallelism are better than five optical fringes and less than a 3 minute arc (1/20 degree), respectively. The quartz plates are washed subsequently by acetone, ethanol and DI water, then dried by dry nitrogen flow.

Thanks to the hydrophobic property of the plates, 0.4 μl polystyrene suspension is dropped on the bottom substrate. Silicone oil is coated on the outer area of the droplet to form a 'corral'. Silica microspheres (diameter 7.75 μm, SD = 0.29 μm, 5wt% aqueous suspension, MicroParticles, Germany) are used as the spacers on the plate edges to separate the two plates.

To prevent the evaporation and the leaking of water throughout the observation, optical adhesive (NOA 63, Norland Products, USA) is useful to seal the cell. The adhesive is exposed by 365 nm ultraviolet light with 3 W power for 3 min. The cell then cools down for about 1 min.

Optical observation. Long working distance optical microcopy (Eclipse LV100, Nikon) with the transition mode and objective lens (50×, CFI, ELWD, NA = 0.55, WD = 9.8 mm) is employed to image the particle motion. A Marlin AVT CCD camera is operating at 60 frames s^{-1} and a resolution of 475 nm pixel^{-1}. The depth of field for the optical system is about 1 μm, which is smaller than the diameter of the particle devoted to good focus on one layer of the particles in the solution. A monolayer of particles located in the middle zone between the two plates has been assured by moving the focal plane of the microscope back and forth between these two plates. As the size of the video file recorded in 100 h far exceeds the storage of the computer disk, and the mean square displacement changes very little in one h due to the system evolving very slowly in 100 h, thus particle motion has been recorded for ten minutes at the beginning of each h, then the illumination is turned off to avoid thermal perturbation on the q2D cell. The temperature during the observation is relatively stable (with the variation less than 2 °C).

Image processing. A plugin [23] in ImageJ from NIH developed by the MOSAIC Group at the Max Planck Institute of Molecular Cell Biology and Genetics is employed to detect the particles and track their motion in the 2D surface. Specific parameters suitable for our system are the following: image imported, 1000 frames; field of view, 256 × 256 pixels; time interval, τ = 16.7 ms; radius of particle, 3 pixels; cut-off, 0; percentile, 2; link-frame, 2 frames; displacement, 1 pixel. By running the plugin, the trajectory for each particle is recognized and recorded as x–y coordinates. The adjacent coordinates are used to calculate the mean

displacement $\langle \Delta x \rangle$ by summing the individual displacements $\Delta X_{i,j}$ and taking the average of all displacements,

$$\Delta X_{i,j} = \left[\left(x_{i,j} - x_{i,j-1} \right)^2 + \left(y_{i,j} - y_{i,j-1} \right)^2 \right]^{0.5}, \tag{A1}$$

where i is the trajectory sequence and j is the position sequence of one particle for its trajectory. Trajectory overlapping is calculated as

$$C_x^i = \frac{1}{n_\mathrm{p}} \sum_{j=1}^{n_\mathrm{p}} x_{i,j};\ C_y^i = \frac{1}{n_\mathrm{p}} \sum_{j=1}^{n_\mathrm{p}} y_{i,j}, \tag{A2}$$

where C_x^i and C_y^i are the center coordinates of the ith trajectory and n_p is the number of positions in a time duration. For example, when particles A and B are very close, their trajectories will overlap as time proceeds, then the position of the center of trajectory A is apart from that of trajectory B within a critical distance d_0. We define

$$d = \left[\left(C_x^i - C_x^{i-1} \right)^2 + \left(C_y^i - C_y^{i-1} \right)^2 \right]^{0.5} \tag{A3}$$

as the distance between the centroids of two trajectories. For each trajectory, we search all its neighbors, and group them in a threshold distance to form a trajectory cluster with the center $\mathrm{O}_m \left(x_m, y_m, z_m \right)$. The value of z_m is the intensity of trajectory overlapping. Then the coordinate of the trajectory cluster is

$$x_m = \frac{1}{N} \sum_{i=1}^{N} C_x^i;\ y_m = \frac{1}{N} \sum_{i=1}^{N} C_y^i, \tag{A4}$$

where N is the number of trajectories grouped in a trajectory cluster, m is the sequence number of trajectory clusters.

$$z_m = \sum_{i=1}^{N} z_i;\ z_i = k \left(d_0 - d \right),\ d < d_0; \quad z_i = 0, \quad d \geqslant d_0. \tag{A5}$$

k is the interaction factor and is set to 10 in the present case, and d_0 is the diameter of a particle, which corresponds to the minimum distance between the centers of two adjacent particles.

Estimation of resolution for particle tracking. The tracking tools [23] employed in the present work has been developed from the work of Croker and Grier [13]. The errors mainly come from the following two aspects [13]. (a) The error resulting from clipping in the displacement of particle position is

$$\Delta_\varepsilon^\mathrm{c} \approx \varepsilon \left(\frac{2w^2}{s^2} \right) \exp\left(-\frac{2w^2}{s^2} \right) \left[1 - \exp\left(-\frac{2w^2}{s^2} \right) \right]^{-1} \tag{A6}$$

in which $\varepsilon = \sqrt{\varepsilon_x^2 + \varepsilon_y^2}$ is a number larger and smaller than the apparent radius (of the particle) in pixels and the interparticle separation, respectively; s is the particle radius in the image. ε_x and ε_y are the deviations from a particle's centroid in x and y directions, respectively,

$$\varepsilon_x = \frac{1}{m_0} \cdot \sum_{\substack{i=-i_m \\ j=-j_m}}^{i_m,j_m} i \cdot A\,(x+i,\, y+j) \tag{A7}$$

$$\varepsilon_y = \frac{1}{m_0} \cdot \sum_{\substack{i=-i_m \\ j=-j_m}}^{i_m,j_m} j \cdot A\,(x+i,\, y+j) \tag{A8}$$

in which

$$m_0 = \sum_{\substack{i=-i_m \\ j=-j_m}}^{i_m,j_m} A\,(x+i,\, y+j) \tag{A9}$$

is the integrated brightness for a particle with $i^2 + j^2 \leqslant w^2$, i, j are integers, i_m, j_m are the maximum values of i, j, respectively, and $A(x,y)$ is the brightness. (b) The error due to the noise in the background brightness:

$$\Delta_\varepsilon^{\mathrm{n}} \approx \left(\frac{\Delta A}{m_0}\right)\left(\frac{2w^2}{s^2}\right)\frac{1}{2\pi^{\frac{1}{2}}}\left[1 - \exp\left(-\frac{2w^2}{s^2}\right)\right]^{-1} \tag{A10}$$

where ΔA is the deviation from m_0 as the background brightness is changing. Thus the total measurement error of the particle tracking is

$$\Delta_\varepsilon = \sqrt{\left(\Delta_\varepsilon^{\mathrm{c}}\right)^2 + \left(\Delta_\varepsilon^{\mathrm{n}}\right)^2}. \tag{A11}$$

Taking the average value of three measurements, $w \approx 3$ pixels, $s = 2.5$ pixels. When the particle has moved for the time of 16.7 ms, we get $m_0 = 3383, 2758, 2683$ and $m'_0 = 3423, 2713, 2651$, respectively, that is $\frac{\Delta A}{m_0} = 0.012, 0.016, 0.026$. Additionally, we get $\varepsilon = \sqrt{\varepsilon_x^2 + \varepsilon_y^2} = 0.073, 0.066, 0.160$, respectively. By using the equations (A6), (A10) and (A11), we have $\Delta_\varepsilon^{\mathrm{c}} \approx 0.011, 0.012, 0.02$, $\Delta_\varepsilon^{\mathrm{n}} \approx 0.010, 0.014, 0.023$, and $\Delta_\varepsilon = 0.02, 0.02, 0.03$, respectively. Therefore, the precision of the particle tracking in the present work, taking the mean value, is $\sim$10 nm.

$\Delta_\varepsilon^{\mathrm{c}}$ and $\Delta_\varepsilon^{\mathrm{n}}$ are random errors, thus the total error Δ_ε is a random error. The uncertainties caused by the random error have equal chances to be positive and negative, where these positive and negative uncertainties would cancel each other [24], [25]. As a large number of measurements are made, the average of the measurements would be very close to the true value [24]. Since the measured numbers of particle trajectories are large, random error tends to cancel out. Therefore, although the above calculation of Δ_ε leads to an uncertainty of $\sim$10 nm, the actual uncertainty could be less than this due to the character of random error for Δ_ε.

Appendix B. Collision rate

The collision rate can be qualitatively analyzed by approximately considering the bulk and q2D suspension as consisting of cube and square zones (with colloidal particles as vertices, figure 1(c) inset), respectively. The number of particles in a cube is $\frac{1}{8} \times 8 = 1$, thus the volume

Table 1. Example of Δx and $\delta(\Delta x) = \Delta x_1 - \Delta x_{95}$.

$\Delta x_1\,(nm)$	94	331	239	93	206	206	155
$\Delta x_{95}\,(nm)$	128	73	254	254	88	3	91
$\delta(\Delta x)\,(nm)$	–34	258	15	–161	118	203	64
$\Delta x_1\,(nm)$	88	204	211	212	147	141	212
$\Delta x_{95}\,(nm)$	91	90	0	14	181	155	2
$\delta(\Delta x)\,(nm)$	–3	114	211	198	–34	–14	210
$\Delta x_1\,(nm)$	147	142	71	331	350	76	
$\Delta x_{95}\,(nm)$	2	0	153	221	7	7	
$\delta(\Delta x)\,(nm)$	145	142	–82	110	343	69	

density of particles $\varrho_b = \frac{4\pi r^3}{3a^3}$, where a is lattice length. After a particle has passed a cube zone, the volume of its path $V_b \approx \pi r^2 a$. So the possibility of the particle colliding with the other particles (at vertices) in a cube, $p_b = \frac{V_b}{a^3}\varrho_b = \frac{4\pi^2 r^5}{3a^5}$. The number of particles in a 2D square area is $\frac{1}{4} \times 4 = 1$, so the area density of particles $\varrho_q = \frac{\pi r^2}{a^2}$. The area of the path corresponding to a particle passing through the square zone, s $S_q \approx 2ra$. Then the possibility of the particle colliding with other particles (at vertices) in a square, $p_q = \frac{S_q}{a^2}\varrho_q = \frac{2\pi r^3}{a^3}$. Thus $p_q/p_b = 0.5\left(\frac{a}{r}\right)^2 \gg 1$ (for dilute suspension). Therefore, as the particle passes the same distance in the suspension, the possibility of particle collision in the q2D confinement is much larger than that in the bulk.

Appendix C. The damping effect

For the N measurements of particle displacement, the difference of the average displacement at the different times is

$$\delta\langle\Delta x\rangle = \langle\Delta x_t\rangle - \langle\Delta x_{t'}\rangle \tag{A12}$$

where t and t' are different times. For the convenience of understanding the damping effect, here we derive an alternative mathematical presentation for $\delta\langle\Delta x\rangle$: $\langle\Delta x_t\rangle - \langle\Delta x_{t'}\rangle = \frac{\Sigma x_t}{N} - \frac{\Sigma x_{t'}}{N} = N^{-1}\left[\left(\Delta x_{t1} - \Delta x_{t'1}\right) + \left(\Delta x_{t2} - \Delta x_{t'2}\right) + \left(\Delta x_{t3} - \Delta x_{t'3}\right) + \ldots + \left(\Delta x_{tN} - \Delta x_{t'N}\right)\right] = N^{-1}\left[\delta\Delta x_1 + \delta\Delta x_2 + \delta\Delta x_3 + \ldots + \delta\Delta x_n\right] = N^{-1}\Sigma\delta\Delta x_k = \langle\delta\Delta x\rangle$, thus,

$$\delta\langle\Delta x\rangle = \langle\delta\Delta x\rangle \tag{A13}$$

Table 1 displays $\triangle x$ and $\delta(\Delta x)$ produced by an arbitrary data sequence at 1 h and 95 h. For table 1, the total sum $\Sigma\delta(\Delta x) = 1872$ nm. From equation (A13), $\delta\langle\Delta x\rangle = \langle\delta\Delta x\rangle = \Sigma\delta(\Delta x)/20 = 94$ nm. For one pair of Δx at different times, the maximum $\delta\Delta x$ in table 1 is 258 nm, whereas for 20 pairs of Δx, the corresponding $\delta\langle\Delta x\rangle$ is 94 nm. Taking into account the huge numbers of Δx in the experimental measurement, we reach the result of $\langle\Delta x\rangle$ displayed in figure 2(a). As shown in figure 2(a), $\delta\langle\Delta x\rangle = 8$ nm is produced from the damping from the beginning (1 h) to the equilibrium (~100 h). These results reflect the fact that

the higher the values of the Δx measurement, the lower the value of $\delta\langle\Delta x\rangle$ is. This means that a reliable value of $\delta\langle\Delta x\rangle$ can only be established on the basis of the statistics of large numbers of $\delta\langle\Delta x\rangle$.

On the other hand, this indicates that, though the average value of large numbers of Δx is small, one or the average of a few Δx is much larger, which reveals that the dynamic change is more obvious than reflected by the average value of large numbers of Δx in figure 2(a). This is well indicated from the above analysis of table 1 by using equation (A13). $\delta\langle\Delta x\rangle = 8$ nm shown in the main text is obtained by using equation (A12), because the total numbers of the Δx at the different times are different and equation (A13) is based on the same numbers of Δx. For the analysis of trajectories in 16.7 ms, the software outputs results which show that the particle number and valid trajectories are 492 and 10 232, 463 and 8508 for 1 h and 95 h, respectively.

Appendix D. Solution of equation (3)

Solving equation (3), we get

$$v = \left(k - 1 + \mathrm{e}^{\gamma t}\right)^{-\frac{\beta}{\gamma}} \left\{ \int_0^t \left[1 + (k-1)\,\mathrm{e}^{-\gamma t}\right]^{\frac{\beta}{\gamma}-1} \mathrm{e}^{\beta t} A(t)\,\mathrm{d}t + C \right\}. \tag{A14}$$

γ is far less than and k is very close to unity, thus $(k-1)\,\mathrm{e}^{-\gamma t} \ll 1$. With series expansion, $\int_0^t \left[1 + (k-1)\,\mathrm{e}^{-\gamma t}\right]^{\frac{\beta}{\gamma}-1} \mathrm{e}^{\beta t} A(t)\,\mathrm{d}t \approx \int_0^t \left[1 + \left(\frac{\beta}{\gamma} - 1\right)(k-1)\,\mathrm{e}^{-\gamma t}\right] \mathrm{e}^{\beta t} A(t)\,\mathrm{d}t = \int_0^t \left[\mathrm{e}^{\beta t} + \left(\frac{\beta}{\gamma} - 1\right)(k-1)\,\mathrm{e}^{(\beta-\gamma)t}\right] A(t)\,\mathrm{d}t$, as $A(t)\,(=F/m)$ is not a function and $\beta \gg \gamma$, thus $\left[1 + (k-1)\,\mathrm{e}^{-\gamma t}\right]^{\frac{\beta}{\gamma}-1}$ can be moved outside the integral symbol with negligible error on the integral value,

$$\int_0^t \left[1 + (k-1)\,\mathrm{e}^{-\gamma t}\right]^{\frac{\beta}{\gamma}-1} \mathrm{e}^{\beta t} A(t)\,\mathrm{d}t \approx \left[1 + (k-1)\,\mathrm{e}^{-\gamma t}\right]^{\frac{\beta}{\gamma}-1} \int_0^t \mathrm{e}^{\beta t} A(t)\,\mathrm{d}t. \tag{A15}$$

For initial conditions $t = 0$ and $v(0) = v_0$, from equation (A14), we obtain $C = k^{\frac{\beta}{\gamma}} v_0$. Substituting C and equation (A15) into equation (A14), we obtain

$$v = v_0 k^{\frac{\beta}{\gamma}} \left(\mathrm{e}^{\gamma t} + k - 1\right)^{-\frac{\beta}{\gamma}} + \frac{\mathrm{e}^{-\beta t}}{1 + (k-1)\,\mathrm{e}^{-\gamma t}} \int_0^t \mathrm{e}^{\beta \xi} A(\xi)\,\mathrm{d}\xi. \tag{A16}$$

Taking the square of equation (A16) and doing the calculation, we get the mean-square velocity $\left\langle v^2 \right\rangle$ as presented in equation (4). Integrating equation (A16) to get the displacement,

$$\Delta x = v_0 k^{\frac{\beta}{\gamma}} \int_0^t \left(e^{\gamma t} + k - 1\right)^{-\frac{\beta}{\gamma}} dt + \int_0^t \frac{e^{-\beta t}}{1 + (k-1)e^{-\gamma t}} dt \int_0^t e^{\beta \xi} A(\xi)\, d\xi. \tag{A17}$$

Due to the slow damping process, $\gamma t < 1$,

$$e^{\gamma t} = 1 + \gamma t + \frac{1}{2}(\gamma t)^2 + \ldots \approx 1 + \gamma t. \tag{A18}$$

With $|(k-1)e^{-\gamma t}| \ll 1$, $\int_0^t \frac{e^{-\beta t}}{1+(k-1)e^{-\gamma t}} dt \approx \int_0^t \left[1 - (k-1)e^{-\gamma t}\right] e^{-\beta t} dt = \int_0^t \left[e^{-\beta t} - (k-1)e^{-(\beta+\gamma)t}\right] dt$, and $\beta \gg \gamma$, thus $\frac{1}{1+(k-1)e^{-\gamma t}}$ can be moved outside the integral symbol with negligible error on the integral value,

$$\int_0^t \frac{e^{-\beta t}}{1 + (k-1)e^{-\gamma t}} dt \approx \frac{1}{1 + (k-1)e^{-\gamma t}} \int_0^t e^{-\beta t} dt. \tag{A19}$$

We substitute equations (A18) and (A19) into the first and second terms of equation (A17), respectively. Integrating the first term and performing integration by parts for the second term, it reaches

$$\Delta x = \frac{k v_0}{\beta - \gamma}\left[1 - \left(\frac{k}{\gamma t + k}\right)^{\frac{\beta}{\gamma}-1}\right] + \frac{1}{\beta\left[1 + (k-1)e^{-\gamma t}\right]} \times \left[-e^{-\beta t}\int_0^t e^{\beta \xi} A(\xi)\, d\xi + \int_0^t A(\xi)\, d\xi\right]. \tag{A20}$$

Squaring equation (A20) and performing the calculation ($\beta \gg \gamma$), we have equation (5).

Appendix E. Derivation and solution of equation (9)

(a) Derivation. Gaveau *et al* derived the probability density of the particle performing the motion in the stochastic process as [18]

$$\frac{\partial^2 P}{\partial t^2} + 2a\frac{\partial P}{\partial t} = v^2 \frac{\partial^2 P}{\partial x^2}. \tag{A21}$$

Here, we derive equation (9) by working out the coefficients a, v in the case of particle motion damping. The velocity of the particle is slowly damped as $v = v_0 e^{-\lambda t}$. Consider that a particle has been persistently bombarded by liquid molecules, with the average number of collisions n_c per unit length of its trajectory. The particle changes the direction of motion after passing an average length of trajectory L, i.e., after $n_c L$ collisions with liquid molecules. The probability of change of the direction of motion in unit time, $a = v/L = v_0 e^{-\lambda t}/L = a_0 e^{-\lambda t}$. Substituting v and a into equation (A21), we get equation (9).

(b) Solution. Setting $P(x, t) = X(x)\,T(t)$ and using the method of separating variables, we convert equation (9) into the following equations:

$$X'' + k_n^2 X = 0, \quad n = 0, 1, 2\ldots \tag{A22}$$

$$T'' + 2a_0 e^{-\lambda t} T' + k_n^2 v_0^2 e^{-2\lambda t} T = 0, \quad n = 0, 1, 2\ldots. \tag{A23}$$

The general solution of equation (A22) is $X = c_1 \cos k_n x + c_2 \sin k_n x$. Using the initial condition $P(0, 0) = X(0) T(0) = 1$, as $T(0) = 1$ (no damping at $t = 0$), $X(0) = 1$, we obtain $X(0) = c_1 = 1$. Furthermore, $\frac{dX}{dx}|_{x=0} = 0$; we have $c_2 k_n = 0$, $c_2 = 0$. In addition, $P(L, 0) = X(L) T(0) = 0$, $X(L) = 0$, so $X(L) = \cos k_n L = 0$, $k_n = \frac{(2n+1)\pi}{2L}$, $n = 0, 1, 2\ldots$. Thus we have

$$X = \cos k_n x. \tag{A24}$$

We realize that $T_1 = e^{-st}$ can be a particular solution of equation (A23). Substituting T_1 into the equation we obtain $s_{1,2} = e^{-\lambda t}\left(a_0 \pm \sqrt{a_0^2 - k_n^2 v_0^2}\right)$. In the case of the damping, we take $s = e^{-\lambda t}\left(a_0 - \sqrt{a_0^2 - k_n^2 v_0^2}\right) = c_0 e^{-\lambda t}$. The second linearly independent solution of equation (A23) is $T_2 = T_1 \int \left(e^{-\int 2a_0 e^{-\lambda t} dt} / T_1^2\right) dt = T_1 \int e^{2e^{-\lambda t}\left(\frac{a_0}{\lambda} + c_0 t\right)} dt$. As λ has similar character to γ in equation (A18), $T_2 \approx T_1 \int e^{2(1-\lambda t)\left(\frac{a_0}{\lambda} + c_0 t\right)} dt = \frac{T_1}{2(c_0 - a_0)} e^{2\left[\frac{a_0}{\lambda} + (c_0 - a_0) t\right]}$. So we obtain

$$T(t) = c_3 T_1 + c_4 T_2 = e^{-c_0 t e^{-\lambda t}}\left(c_3 + c_5 e^{-\rho t}\right) \tag{A25}$$

where $c_5 = \frac{c_4}{2(c_0 - a_0)} e^{\frac{2a_0}{\lambda}}$, $\rho = 2\sqrt{a_0^2 - k_n^2 v_0^2}$, $c_0 = a_0 - \sqrt{a_0^2 - k_n^2 v_0^2}$. The probability density in an interval $[x, x + dx]$ on a line of length L is proportional to the numbers counted for a particle lying in $[x, x + dx]$. The higher the velocity is for the particle, the more counts it has in unit time, i.e. $P \propto v$. The ratio of probability density for $t \to \infty$ to that for $t = 0$, $\frac{P(x,\infty)}{P(x,0)} = \frac{X(x) T(\infty)}{X(x) T(0)} = \frac{T(\infty)}{T(0)} = \frac{v_e}{v_0}$, where v_e is the velocity at the final equilibrium state as $t \to \infty$. Since $\lim_{t\to\infty} - c_0 t e^{-\lambda t} = \lim_{t\to\infty} \frac{-c_0 t}{e^{\lambda t}} = 0$, from equation (A25), $T(\infty) = c_3 = v_e / v_0$. For the initial condition $T(0) = c_3 + c_5 = 1$, $c_5 = 1 - \frac{v_e}{v_0}$. We obtain

$$T(t) = v_0^{-1} e^{-c_0 t e^{-\lambda t}}\left[v_e + (v_0 - v_e) e^{-\rho t}\right]. \tag{A26}$$

From equations (A24) and (A26), we thus arrive at the product solution equation (10).

References

[1] Huang M-J, Chen H-Y and Mikhailov A S 2012 *Eur. Phys. J.* E **35** 119
[2] Tan M, Le D and Chiam K 2012 *Soft Matter* **8** 2243
[3] Bonilla-Capilla B, Ramírez-Saito A, Ojeda-López M and Arauz-Lara J 2012 *J. Phys.: Condens. Matter* **24** 464126
[4] Novikov S, Rice S A, Cui B, Diamant H and Lin B 2010 *Phys. Rev.* E **82** 031403
[5] Uspal W E and Doyle P S 2012 *Phys. Rev.* E **85** 016325
[6] Uspal W E and Doyle P S 2012 *Soft Matter* **8** 10676
[7] Nugent C R, Edmond K V, Patel H N and Weeks E R 2007 *Phys. Rev. Lett.* **99** 025702
[8] Edmond K V, Nugent C R and Weeks E R 2012 *Phys. Rev.* E **85** 041401
[9] Eral H B, van den Ende D, Mugele F and Duits M H G 2009 *Phys. Rev.* E **80** 061403
[10] Carbajal-Tinoco M, de León G and Arauz-Lara J 1997 *Phys. Rev.* E **56** 6962

[11] Cui B, Diamant H, Lin B and Rice S A 2004 *Phys. Rev. Lett.* **92** 258301
[12] Diamant H 2009 *J. Phys. Soc. Jpn.* **78** 041002
[13] Crocker J C and Grier D G 1996 *J. Colloid Interface Sci.* **179** 298
[14] Uhlenbeck G E and Ornstein L S 1930 *Phys. Rev.* **36** 823
[15] Batchelor G and Green J 1972 *J. Fluid Mech.* **56** 375
[16] Peyla P and Verdier C 2011 *EPL* **94** 44001
[17] Einstein A 1956ed R Fürth *Investigations on the Theory of the Brownian Movement* (New York: Dover)
[18] Gaveau B, Jacobson T, Kac M and Schulman L S 1984 *Phys. Rev. Lett.* **53** 419
[19] Cahn J W 1965 *J. Chem. Phys.* **42** 93
[20] Vrij A 1966 *Discuss Faraday Soc.* **42** 23
[21] Pierański P, Małecki J, Kuczyński W and Wojciechowski K 1978 *Philos. Mag.* **37** 107
[22] Türkcan S, Alexandrou A and Masson J-B 2012 *Biophys. J.* **102** 2288
[23] Sbalzarini I F and Koumoutsakos P 2005 *J. Struct. Biol.* **151** 182
[24] Babbage C Error Analysis and Significant Figures. http://owlnet.rice.edu/~labgroup/pdf/Error_analysis.htm
[25] Taylor J R 1997 *An Introduction to Error Analysis: the Study of Uncertainties in Physical Measurements* (Sausalito, CA: University Science Books)